CHAPTER

8

On-section correlative light and electron microscopy of large cellular volumes using STEM tomography

Korbinian Buerger[a,*,†], Kerstin N. Schmidt[a,†], Jantina Fokkema[b], Hans C. Gerritsen[b], Olga Maier[a], Uwe de Vries[a], Yulia Zaytseva[a], Reinhard Rachel[c], and Ralph Witzgall[a,*]

[a]*Institute for Molecular and Cellular Anatomy, University of Regensburg, Regensburg, Germany*
[b]*Molecular Biophysics, Debye Institute for Nanomaterials Science, Utrecht University, Utrecht, The Netherlands*
[c]*Center for Electron Microscopy, University of Regensburg, Regensburg, Germany*
**Corresponding authors: e-mail address: korbinian.buerger@vkl.uni-regensburg.de; ralph.witzgall@vkl.uni-regensburg.de*

Chapter outline

[†]Shared first authorship.

Methods in Cell Biology, Volume 162, ISSN 0091-679X, https://doi.org/10.1016/bs.mcb.2020.09.002

Abstract

The application of both fluorescence and electron microscopy results in a powerful combination of imaging modalities called "correlative light and electron microscopy" (CLEM). Whereas conventional transmission electron microscopy (TEM) tomography is only able to image sections up to a thickness of ~300 nm, scanning transmission electron microscopy (STEM) tomography at 200 kV allows the analysis of sections up to a thickness of 900 nm in three dimensions. In the current study we have successfully integrated STEM tomography into CLEM as demonstrated for human retinal pigment epithelial 1 (RPE1) cells expressing various fluorescent fusion proteins which were high-pressure frozen and then embedded in

Lowicryl HM20. Fluorescently labeled gold nanoparticles were applied onto resin sections and imaged by fluorescence and electron microscopy. STEM tomograms were recorded at regions of interest, and overlays were generated using the eC-CLEM software package. Through the nuclear staining of living cells, the use of fluorescently labeled gold fiducials for the generation of overlays, and the integration of STEM tomography we have markedly extended the application of the *Kukulski protocol* (Kukulski et al., 2011, 2012). Various fluorescently tagged proteins localizing to different cellular organelles could be assigned to their ultrastructural compartments. By combining STEM tomography with on-section CLEM, fluorescently tagged proteins can be localized in three-dimensional ultrastructural environments with a volume of at least $2.7 \times 2.7 \times 0.5\,\mu m$.

1 Introduction

Fluorescence microscopy and electron microscopy are the two most important imaging modalities for research in the life sciences (de Boer, Hoogenboom, & Giepmans, 2015; Giepmans, 2008). Both imaging methods have their own advantages and disadvantages. Molecules and thus cellular structures can be fluorescently labeled using various techniques and subsequently be identified by fluorescence microscopy (Giepmans, 2008). Moreover, when live-cell imaging is performed dynamic cellular processes can be imaged (de Boer et al., 2015). Using super-resolution microscopy, it is even possible to overcome the diffraction limit posed by Ernst Abbe (de Boer et al., 2015; Hell & Wichmann, 1994; Yang et al., 2018). However, a major disadvantage of fluorescence microscopy remains that sub-cellular structures cannot be visualized simultaneously (de Boer et al., 2015; Giepmans, 2008). This is the advantage of electron microscopy by which cellular ultrastructure can be imaged with a resolution in the nanometer range. In addition, when electron tomographic methods are applied, the cellular context can be characterized even in three dimensions (McIntosh, Nicastro, & Mastronarde, 2005; Noske, Costin, Morgan, & Marsh, 2008; Saghi & Midgley, 2012). Correlative light and electron microscopy (CLEM) is the combination of these two imaging modalities (de Boer et al., 2015). By combining fluorescence and electron microscopy, a variety of options arise to investigate cellular processes at a new level (Giepmans, 2008).

One of the first attempts to combine the advantages of light and electron microscopy was published by Kobayashi, Serizawa, Fujita, and Coupland (1978) who performed silver impregnation of Epon 812 sections using an ammoniacal silver solution to stain structures of interest (Kobayashi et al., 1978). Strictly speaking, however, the authors did not follow a "true" CLEM approach as different sections of the samples were imaged, i.e., ultra-thin sections by electron microscopy and semi-thin sections by light microscopy (Kobayashi et al., 1978). Biel et al. achieved this milestone in 2003 when high-pressure freezing of human skin biopsies was followed by freeze-substitution in the presence of different fluorescent dyes. Applying this procedure, the authors succeeded to image the same object by both light and

electron microscopy (Biel, Kawaschinski, Wittern, Hintze, & Wepf, 2003). Since 2003, a variety of different CLEM protocols have been developed (de Boer et al., 2015). There are different possibilities to classify these techniques. One option is to categorize CLEM procedures according to whether fluorescence microscopy is performed before (pre-embedding CLEM) or after sample preparation for electron microscopy (on-section CLEM) (de Boer et al., 2015; Santarella-Mellwig et al., 2018). Both approaches have their advantages and disadvantages. In on-section CLEM experiments, for example, a compromise between fluorescence and ultrastructure preservation must be made (Kukulski et al., 2012). Therefore, this method is not suitable for all biological research questions. The advantage of on-section CLEM, however, is that there is no time lag between both imaging modalities (Kukulski et al., 2012). In addition, there is a high correlation accuracy of at least 30 nm, possibly up to 5 nm, between the fluorescence and the electron microscopic images (Mohammadian et al., 2019). In 2011, Kukulski et al. published an on-section CLEM approach preserving the fluorescence intensity of fluorescent proteins in Lowicryl HM20 (Kukulski et al., 2011). The main steps of this procedure are high-pressure freezing, freeze-substitution using a cocktail of 0.1% (w/v) uranyl acetate in acetone, followed by Lowicryl HM20 embedding. After generating 300 nm sections, the fluorescence signals of the fluorescent proteins EGFP and mCherry could be detected by fluorescence microscopy at room temperature. Subsequently, tomograms of the regions previously documented by fluorescence microscopy were recorded using a transmission electron microscope (TEM). In a final step, fluorescence and electron microscopic data could be correlated with an accuracy of less than 100 nm due to the use of fluorescent fiducial markers (FluoSpheres) (Kukulski et al., 2012). Initially limited to room temperature fluorescence microscopy, this method was later adapted to low temperatures so that samples could be imaged in a more native state (Schorb et al., 2017). For this purpose not only a cryo-electron microscope was used but also a fluorescence microscope had to be developed to image the sample under liquid nitrogen conditions (Schorb et al., 2017).

Depending on the scientific question asked, different cellular components are of interest. The size of cellular structures varies from a few nanometers to several micrometers in diameter. In CLEM experiments, the limiting factor regarding the investigation of large volumes is electron microscopy. To reconstruct the third dimension, a variety of techniques for electron microscopes have been developed (Karreman et al., 2016; Markert et al., 2016; Sartori-Rupp et al., 2019). Recently scanning transmission electron microscopy (STEM) tomography at 200 kV was adapted so that cellular structures in up to 900 nm thick resin sections could be visualized in three dimensions (Biskupek, Leschner, Walther, & Kaiser, 2010; Rachel et al., 2020; Sousa & Leapman, 2012). We succeeded in implementing this imaging technique in a conventional 200 kV TEM, thus avoiding the problem of spherical aberration during the imaging process (Rachel et al., 2020). By using a TEM with a field emission gun and an electron beam with a low semi-convergence angle of about 1–2 mrad, a high depth of focus was achieved, sufficient to visualize

900 nm thick samples also at high tilt angles of up to ±72° (Rachel et al., 2020). The major advantage of this technique is the ability to visualize large cellular volumes ($2.7 \times 2.7 \times 0.9\,\mu m$) in combination with a high resolution in the z axis of about 5–10 nm (Rachel et al., 2020).

Ader and Kukulski combined STEM tomography with on-section CLEM (Ader & Kukulski, 2017). These authors imaged resin sections with a nominal thickness of 300 nm during their CLEM-STEM approach (Ader & Kukulski, 2017). Using an optimized setting, however, STEM tomography makes it possible to visualize much thicker samples in three dimensions (Rachel et al., 2020). Until now, STEM tomography using an electron beam with a small convergence angle has not been used for CLEM experiments. As STEM tomography was implemented in a TEM, sample preparation should be in general identical to those of the *Kukulski protocol*. However, some steps of this protocol needed to be optimized for thick resin sections. Here, we present a streamlined and improved protocol by which cellular structures of interest can be identified in large volumes by fluorescence microscopy and subsequent STEM tomography in the nanometer range.

2 Methods

2.1 Molecular cloning

miniSOG and SmoM2 cDNAs were amplified via PCR. A SmoM2-miniSOG-mCherry construct was generated by cloning miniSOG and SmoM2 into the mammalian expression plasmid pmCherry-N1 using the restriction enzymes *Sac*II/*Age*I for miniSOG and *Eco*RI/*Sal*I sites for SmoM2. The construct (pSmoM2, miniSOG, mCherry) was confirmed by restriction digest and Sanger sequencing.

2.2 Cell lines

All cell lines were cultured at 5% CO_2 and 37 °C in DMEM/Ham's F12 medium with the addition of 10% FCS, 2 mM L-glutamine and 0.26% sodium bicarbonate. Transient transfections with plasmid DNA were performed using FuGENE 6. For generating the stably transfected cell line producing Centrin1-GFP and SmoM2-miniSOG-mCherry, RPE1 cells already producing Centrin1-GFP were co-transfected with SmoM2-miniSOG-mCherry and the puromycin-resistance expression plasmid pWE 3. Selection was performed using 2 µg/mL of puromycin for approximately 2 weeks. All clones were trypsinized and FACS-sorted for GFP and mCherry signals. To generate a monoclonal cell line after FACS sorting, limiting dilution was performed by seeding cells at a concentration of 0.5 cells/well in 96-well plates. Clones were chosen based on a bright mCherry signal at the primary cilium by fluorescence microscopy. It was ensured by PCR that all cell lines used in this work were free of mycoplasma contamination.

2.3 Live-cell nuclear staining with different bisBenzimide dyes

Optimal conditions to obtain strong and persistent fluorescent nuclear staining for CLEM were established by carrying out live-cell imaging experiments. 3×10^5 RPE1 cells producing Centrin1-GFP were seeded per 35 mm petri dish. Twenty-four hours after plating, cells were serum-starved for 24 h and then transferred to an inverted fluorescence microscope before the medium was replaced with fresh serum-free medium. bisBenzimide H 33342 or bisBenzimide H 33258 were added to the medium to achieve a final concentration of 18 and 89 μM, respectively. Live-cell imaging was carried out at 37 °C and 5% CO_2. *Z* stacks (nine steps, 3.0 μm each) were recorded every 30 s using a cooled sCMOS camera, a Fluar 20 ×/0.75 objective and a D 350/50 excitation, ET 460/50 emission filter. The microscope was controlled by the VisiView software version 4.1.0.4.

2.4 Sample preparation for CLEM

2.4.1 Cell culture

Cells were either chemically fixed or high-pressure frozen. For chemical fixation, cells were grown on 10-mm glass coverslips; for high-pressure freezing, cells were grown on sapphire discs with a diameter of 1.4 mm and a thickness of 0.05 mm. The sapphire discs were pretreated as follows: 10 min incubation in 32% HCl, 10 min incubation in 70% ethanol and finally 10 min incubation in absolute ethanol. After the removal of ethanol the sapphire discs were air-dried and finally autoclaved. Up to 10 sapphire discs together with one 10-mm glass coverslip were placed in a 35-mm cell culture dish. To facilitate the attachment of cells, sapphire discs were placed into a 2–3 μL drop of FCS, covered with additional FCS and then allowed to dry at room temperature. Finally, the sapphire discs in the dish were dried at 60 °C for 10 min and plasma cleaned for 2 min (RF level High).

In the case of stably transfected RPE1 cells constitutively producing Centrin1-GFP and SmoM2-miniSOG-mCherry, cells were plated at a density of 2×10^5 cells per 35-mm culture dish onto sapphire discs and coverslips. Two days later the cells were washed and cultured in serum-free medium for 72 h to induce ciliogenesis. Prior to fixation for CLEM experiments, cells were stained using 89 μM bisBenzimide H 33342 in medium without FCS at 37 °C and 5% CO_2 for at least 5 min and then fixed for CLEM experiments as described below. When analyzing the trafficking of the FGF receptor 1 RPE1 cells were plated at a density of 2.5×10^5 cells per 35-mm cell culture dish onto sapphire discs and coverslips. Twenty-four hours later they were transiently transfected with an expression plasmid encoding a fusion protein between the FGF receptor 1 at the NH_2-terminus and mNeonGreen at the COOH-terminus. Another 24 h later cells were stained with 89 μM bisBenzimide H 33342 in medium with 10% FCS for 5 min at 37 °C and 5% CO_2. After removal of the bisBenzimide H 33342 solution, cells were washed twice before being high-pressure frozen or fixed chemically.

2.4.2 High-pressure freezing and freeze-substitution

Sapphire discs were placed in membrane carriers together with a drop of FCS, covered with another drop of FCS and high-pressure frozen. The discs were stored in liquid nitrogen until further processing.

The freeze-substitution scheme used in this study is based on the *Kukulski protocol* (Kukulski et al., 2012) and was further optimized for easier correlation between the light and electron microscopic images. Samples were automatically freeze-substituted using the pipetting robot of the EM AFS2. The freeze-substitution cocktail contained 0.1% (w/v) uranyl acetate and 5% water in pure acetone. Sapphire discs were placed on the frozen freeze-substitution solution for which the specimen chamber of the EM AFS2 was pre-cooled to −140 °C. The temperature was raised from −140 °C to −90 °C (slope: 25 °C/h) so that the sapphire discs could sink to the bottom. Thereafter, the procedure was continued as described in Table 1.

2.4.3 Chemical fixation and progressive lowering of temperature

Samples were fixed chemically using 4% formaldehyde in 1 × PBS (either pH 7.4 or 11) for 5 min at 22 °C and then for 55 min on ice. After fixation coverslips were transferred to the lids of snap cap vials, and the samples were dehydrated using a progressive lowering of temperature protocol (Carlemalm, Garavito, & Villiger, 1982; Robertson, Monaghan, Clarke, & Atherton, 1992): 30 min in 30% ethanol

Table 1 Freeze-substitution protocol as in Kukulski et al. (2012), except for the 9 h long incubation in step 1.

Step	T_{start} [°C]	T_{end} [°C]	Slope [°C/h]	Time [hh:mm]	Solution	UV
1	−90	−90	0	09:00	FS medium	–
2	−90	−45	5	09:00	FS medium	–
3	−45	−45	0	05:00	FS medium	–
4	−45	−45	0	00:10	Acetone, 100%	–
5	−45	−45	0	00:10	Acetone, 100%	–
6	−45	−45	0	00:10	Acetone, 100%	–
7	−45	−45	0	02:00	Lowicryl HM20, 10%	–
8	−45	−45	0	02:00	Lowicryl HM20, 25%	–
9	−45	−35	5	02:00	Lowicryl HM20, 50%	–
10	−35	−25	5	02:00	Lowicryl HM20, 75%	–
11	−25	−25	0	10:00	Lowicryl HM20, 100%	–
12	−25	−25	0	10:00	Lowicryl HM20, 100%	–
13	−25	−25	0	10:00	Lowicryl HM20, 100%	–
14	−25	−25	0	48:00	Lowicryl HM20, 100%	+
15	−25	+20	5	09:00	Lowicryl HM20, 100%	+

Freeze-substitution (FS) medium: pure acetone with 5% water and 0.1% (w/v) uranyl acetate. Lowicryl HM20 was diluted with acetone.

at 0 °C, followed by 30 min each in 50% and 70% ethanol at −20 °C. Then the lids with the coverslips were transferred to the specimen chamber of the freeze-substitution unit EM AFS2 and further processed as follows: 30 min in 95% ethanol at −35 °C, two times 30 min in absolute ethanol at −35 °C, 30 min in pure acetone from −35 °C to −40 °C (slope: 10 °C/h), 30 min in pure acetone from −40 °C to −45 °C (slope: 10 °C/h) and finally 3 h in pure acetone from −45 °C to −90 °C (slope: 15 °C/h). Thereafter, samples were further freeze-substituted in a manual fashion as described in Table 1.

2.4.4 Ultramicrotomy

After polymerization, glass coverslips and sapphire discs were removed together with the flat specimen carriers using a razor blade after alternately submerging the resin blocks in liquid nitrogen and water at room temperature (for fluorescence preservation). Lowicryl HM20 discs obtained with the progressive lowering of temperature method were cut into smaller pieces using a razor blade, then individual pieces were mounted on dummy resin blocks and trimmed with a razor blade. Lowicryl HM20 blocks of high-pressure frozen, freeze-substituted samples were trimmed directly with a razor blade. Ultrathin and semi-thin sections were cut parallel to the basal surface of the cell monolayer. To evaluate the preservation of ultrastructural details, 80–90 nm thick sections were collected on Pioloform-coated slot grids. For CLEM-STEM tomography, sections with a nominal thickness of 900 nm were collected on 200 mesh carbon-coated finder copper grids. Fluorescence microscopy of resin sections was performed on the same day as the sections were generated to avoid loss of the fluorescence signal. Only the very first sections of the embedded cells were used as these sections contained the structures of interest.

2.5 Fluorescence microscopy of resin sections

Prior to fluorescence microscopy, rhodamine B-labeled gold nanoparticles (total diameter: 100 nm, diameter of gold core: 15 nm) (Fokkema et al., 2018) were applied to the Lowicryl HM20 sections of high-pressure frozen, freeze-substituted wild-type RPE1 cells transiently synthesizing a fusion protein of the FGF receptor 1 with mNeonGreen. Gold nanoparticles were diluted 1:50 in H_2O (to a final concentration of ~10 µg/mL) and sonicated for 15 min in a water bath. Grids were incubated upside down for 10 min on a 20-µL droplet of the particle suspension before being washed three times with H_2O, blotted with filter paper and dried at 30 °C for ~30 min prior to fluorescence microscopy.

For fluorescence microscopy with oil immersion objectives, grids were mounted between a glass slide and a coverslip with H_2O. Rapid imaging was necessary to prevent the samples from drying out. *Z* stacks (17, 21 or 27 focus steps, 0.4 µm each) of relevant positions were recorded at 22 °C using an inverted light microscope equipped with the required filters. Additional bright-field images were recorded for some positions to facilitate re-orientation at the beginning of electron microscopy. After fluorescence microscopy, glass slides and coverslips were removed, the grids were dried with a filter paper and stored in the dark for further electron microscopy.

2.6 Transmission electron microscopy

To examine the ultrastructural preservation of the specimen, 80–90 nm thick sections were imaged using a transmission electron microscope (TEM) operated at 120 kV. Images were recorded at a pixel size of 0.93 nm.

2.7 Scanning transmission electron microscopy (STEM) and electron tomography

After fluorescence microscopy, a 2–3 nm thick carbon layer was applied to all sections to increase the electrical conductivity for STEM tomography. For this purpose, a high vacuum 208carbon Carbon Coater was operated at 3.6 V for 30 s in an indirect manner (i.e., a shield protected the samples from direct exposure to the evaporated carbon). Then colloidal protein A-gold particles with a diameter of 15 nm were applied as fiducial markers for electron tomography to both sides of the grids. In a last step, the grids were plasma cleaned for 30–40 s (at RF level LOW) and immediately transferred to the electron microscope.

Scanning of grids was performed in the TEM mode using a field emission electron microscope operated at 200 kV to re-locate the regions previously documented by fluorescence microscopy. In TEM mode, the micrographs were recorded using a TemCam F416 camera operated with the software EM-MENU 4. In parallel, the software TvipsCLEM was used to obtain an initial overlay of the fluorescence and electron micrographs for better orientation. The TvipsCLEM software was installed on the same computer controlling the beam and the goniometer to acquire the images. Once the regions of interest were identified, bright-field electron micrographs were recorded in STEM mode (at a low semi-convergence angle of about 1–2 mrad) by running the electron microscope with a Universal Scan Generator and the software EM-TOOLS. Subsequently, tilt series were recorded (pixel size: 1.34 nm) by STEM tomography (electron beam with small convergence angle) at regions of interest. The field of view was ~2.7 µm in both the x and y direction. Ideally, series of 90 images (−66° to +66°) with non-linear increment (Rachel et al., 2020; Saxton, Baumeister, & Hahn, 1984) were recorded.

2.8 Data analysis and overlay generation using eC-CLEM

Fluorescence and electron microscopic images were processed using ImageJ and Adobe Photoshop CS5. ImageJ was also used for the quantification of fluorescence intensity after live-cell staining with different nuclear dyes. Maximum intensity projections of z stacks were generated and thresholding was performed similarly for all time points. Nuclei were counted at one single time point. The total fluorescence intensity of all nuclei was measured at each time point and divided by the number of nuclei.

3D reconstructions were obtained using the IMOD software package using the SIRT (simultaneous iterative reconstruction technique) algorithm (number of iterations: 15). The voxel size of reconstructed tomograms was $1.34 \times 1.34 \times 1.34$ nm. The 15-nm colloidal protein A-gold fiducials were computationally removed using IMOD.

Overlays of fluorescence microscopic images with 2D STEM images and 3D STEM tomograms were generated using the open access software eC-CLEM. The correlation accuracy (in nm) was calculated and documented for each overlay.

3 Instrumentation and materials

3.1 Molecular cloning

Reagents:

Expression plasmid pmNeonGreen/FGFR1 encoding a fusion protein between the fibroblast growth factor receptor 1 (FGFR1) at the NH_2-terminus and mNeonGreen (Shaner et al., 2013) at the COOH-terminus (Peter Claus, MHH Hannover, Germany); complementary DNA (cDNA) of the constitutively active M2 mutant of murine Smoothened (SmoM2) (Chen, Taipale, Cooper, & Beachy, 2002; Incardona, Gruenberg, & Roelink, 2002) (Rajat Rohatgi, Stanford University, USA); miniSOG-C1 (Michael Davidson, Addgene plasmid # 54821; http://n2t.net/addgene:54821; RRID:Addgene_54821) (Shu et al., 2011); expression plasmid pmCherry-N1 (Clontech).

3.2 Cell lines

Instrumentation:

BD FACSAria™ IIu cell sorting system (Becton Dickinson GmbH, Heidelberg, Germany) operating with a 488 nm laser together with a 530/30 filter for EGFP and a 610/20 filter for mCherry.

Reagents:

Human telomerase reverse transcriptase (hTERT)-immortalized retinal pigment epithelial (RPE1) cells and RPE1 cells stably expressing human Centrin1-EGFP (RPE1/Centrin1-GFP) (Uetake et al., 2007) (Gislene Pereira, Center for Organismal Studies, University of Heidelberg, Germany); DMEM/Ham's F12 medium (cat. no. D6421, Sigma-Aldrich, St. Louis, MO, USA) with the addition of 10% FCS (cat. no. P30-3306, PAN-Biotech GmbH, Aidenbach, Germany), 2 mM L-glutamine (cat. no. G7513, Sigma-Aldrich, St. Louis, MO, USA) and 0.26% sodium bicarbonate (cat. no. S8761, Sigma-Aldrich, St. Louis, MO, USA); FuGENE 6 (cat. no. E2691, Promega GmbH, Walldorf, Germany); pWE 3 (Cockett, Ochalski, Benwell, Franco, & Wardwell-Swanson, 1997); puromycin (cat. no. P8833, Sigma-Aldrich, St. Louis, MO, USA).

3.3 Live-cell nuclear staining with different bisBenzimide dyes

Instrumentation:

Inverted fluorescence microscope (Axiovert 200M, Carl Zeiss AG, Oberkochen, Germany) with a HXP 120 V Compact Light Source (Leistungselektronik JENA GmbH, Jena, Germany); CO_2-Controller 2000 (PeCon GmbH, Erbach, Germany); cooled sCMOS camera (pco.edge 4.2, PCO AG, Kelheim, Germany); Fluar 20 ×/0.75

objective (Carl Zeiss AG, Oberkochen, Germany); D 350/50 excitation, ET 460/50 emission filter; VisiView software version 4.1.0.4 (Visitron Systems GmbH, Puchheim, Germany).

Reagents:

bisBenzimide H 33342 (cat. no. 14533, Sigma-Aldrich, St. Louis, MO, USA); bisBenzimide H 33258 (cat. no. B2883, Sigma-Aldrich, St. Louis, MO, USA).

3.4 Sample preparation for CLEM

3.4.1 Cell culture

Instrumentation:

Plasma cleaner PDC-3XG (Harrick Plasma Inc., Ithaca, NY, USA).

Materials:

Ten-mm glass coverslips (cat. no. 631-1576P, VWR International GmbH, Darmstadt, Germany); sapphire discs with a diameter of 1.4 mm and a thickness of 0.05 mm (cat. no. 454, Engineering Office M. Wohlwend GmbH, Sennwald, CH); 35-mm cell culture dish (TC Dish 35 Standard, cat. no. 83.3900, Sarstedt AG & Co. KG, Nümbrecht, Germany).

Reagents:

32% HCl; ethanol.

3.4.2 High-pressure freezing and freeze-substitution

Instrumentation:

EM PACT2 with rapid transfer system RTS (Leica Microsystems GmbH, Wetzlar, Germany); EM AFS2 with pipetting robot (Leica Microsystems GmbH, Wetzlar, Germany).

Materials:

Membrane carriers (cat. no. 1094, Engineering Office M. Wohlwend GmbH, Sennwald, CH); bayonet pods (cat. no. 16707829, Leica Microsystems GmbH, Wetzlar, Germany); manual bayonet loading devices (cat. no. 16707828, Leica Microsystems GmbH, Wetzlar, Germany).

Reagents:

Acetone; uranyl acetate; liquid nitrogen; Lowicryl HM20 (cat. no. 15924-1, Polysciences, Inc., Warrington, PA, USA).

3.4.3 Chemical fixation and progressive lowering of temperature

Materials:

Lids of snap cap vials (cat. no. 548-0623, VWR International GmbH, Darmstadt, Germany).

3.4.4 Ultramicrotomy

Instrumentation:

Ultramicrotome EM UC6 (Leica Microsystems GmbH, Wetzlar, Germany); diamond knife (histo 45°, cat. no. DH4560, Diatome Ltd., Nidau, CH).

Materials:

Razor blade; dummy resin blocks (cat. no. 10580, Plano GmbH, Wetzlar, Germany); Pioloform-coated slot grids (cat. no. G2500C, Plano GmbH, Wetzlar, Germany); 200 mesh carbon-coated finder copper grids (cat. no. S160-H2, Plano GmbH, Wetzlar, Germany).

Reagents:

Super glue (cat. no. 45570, UHU GmbH, Bühl, Germany).

3.5 Fluorescence microscopy of resin sections

Instrumentation:

Inverted light microscope (Zeiss Axiovert 200M) with a HXP 120 V Compact Light Source (Leistungselektronik JENA GmbH, Jena, Germany); Fluar 40 ×/1.30 oil immersion objective (Carl Zeiss AG, Oberkochen, Germany); cooled pco.edge 4.2 sCMOS camera (PCO AG, Kelheim, Germany); VisiView software package (version 4.1.0.4); filter D 350/50 excitation and ET 460/50 emission; filter ET 470/40 excitation and ET 525/50 emission; filter ET 560/40 excitation and ET 630/75 emission.

Materials:

Rhodamine B-labeled gold nanoparticles (Fokkema et al., 2018); coverslips (cat. no. 0107032, high precision, No. 1.5H, Paul Marienfeld GmbH & Co. KG, Lauda-Königshofen, Germany).

3.6 Transmission electron microscopy

Instrumentation:

Transmission electron microscope CM12 (Thermo Fisher Scientific/FEI Co., Eindhoven, The Netherlands) operated at 120 kV under control of the software EM-MENU 4 (TVIPS GmbH, Gauting, Germany); slow-scan CCD camera (TVIPS GmbH, Gauting, Germany).

3.7 Scanning transmission electron microscopy (STEM) and electron tomography

Instrumentation:

High vacuum 208carbon Carbon Coater (Cressington Scientific Instruments, Watford, UK); PDC-3XG plasma cleaner (Harrick Plasma Inc., Ithaca, NY, USA); 200 kV JEM-2100F field emission electron microscope (JEOL GmbH, Freising, Germany) operated with the software EM-MENU 4 (TVIPS GmbH, Gauting, Germany); TemCam F416 camera (TVIPS GmbH, Gauting, Germany); TvipsCLEM software package (TVIPS GmbH, Gauting, Germany); Universal Scan Generator (TVIPS GmbH, Gauting, Germany); EM-TOOLS software package version 1.9.7.2 (TVIPS GmbH, Gauting, Germany); STEM bright-field detector (JEOL GmbH, Freising, Germany).

Materials:

Colloidal protein A-gold with a diameter of 15 nm (cat. no. FG 15 nm, University Medical Center Utrecht).

3.8 Data analysis and overlay generation using eC-CLEM

Materials:

ImageJ software package (National Institutes of Health, Bethesda, MD, USA) (Rueden et al., 2017; Schindelin et al., 2012); Adobe Photoshop CS5 software package (Adobe Inc., San José, CA, USA); IMOD software package version 4.10.23 or later (Kremer, Mastronarde, & McIntosh, 1996); eC-CLEM software package (Paul-Gilloteaux et al., 2017) as a plugin of the Icy software package (de Chaumont et al., 2012).

4 Results

4.1 bisBenzimide H 33342 is a suitable nuclear fluorescent dye to stain living cells for on-section CLEM

CLEM techniques require the identification of the same structure within a given cell, first by fluorescence and subsequently by electron microscopy. For that purpose, prominent landmarks are needed such as the nucleus when nuclear staining or the centrosome when a fluorescent centrosomal marker are present. In order to achieve a satisfying nuclear staining for fluorescence microscopy, two commercially available DNA dyes—bisBenzimide H 33342 and H 33258—were tested as both were reported to be membrane-permeable. Results of live-cell imaging experiments are shown in Fig. 1. Both dyes were taken up by viable cells. As expected, a higher concentration ($c = 89\,\mu M$) resulted in higher fluorescence intensity than a lower one ($c = 18\,\mu M$). Although both dyes are membrane-permeable according to the manufacturer, their staining behavior is different. bisBenzimide H 33342 showed a rapid increase in fluorescence intensity just a few seconds after its addition which was not observed for bisBenzimide H 33258 for either concentration. After a sharp increase in intensity for about 5 min, the fluorescence signal for bisBenzimide H 33342 quickly reached a plateau. During the plateau phase, the fluorescence intensity obtained with bisBenzimide H 33342 at the higher concentration was eight times higher than that obtained with bisBenzimide H 33258. When cells were incubated in bisBenzimide-containing medium longer than 15–20 min, both dyes showed cytotoxic effects. We observed a shrinking of the cells and then a detachment from the culture dish. These effects were observed in a concentration-dependent manner and occurred earlier and to a much greater extent for bisBenzimide H 33342. However, cells could be kept in culture for at least 2 h without showing morphological signs of cytotoxicity when the bisBenzimide-containing medium was replaced by bisBenzimide-free medium after 5 min. Despite culturing the cells in

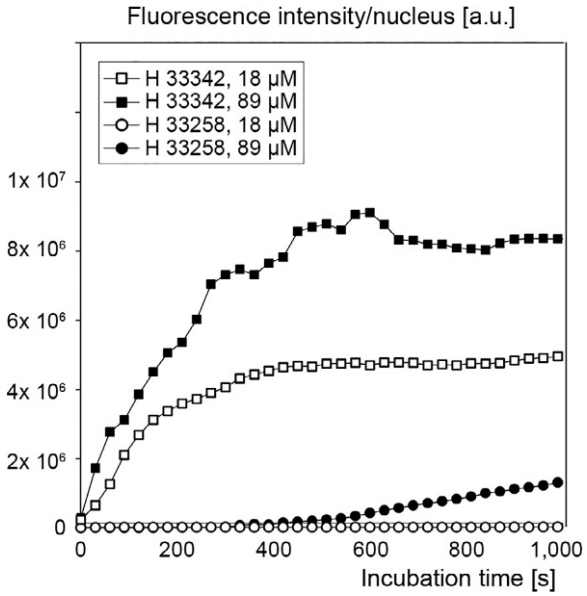

FIG. 1

Uptake of bisBenzimide H 33342 and 33258 into the nuclei of living cells. RPE1 cells were serum-starved for 24 h prior to the addition of the dyes. Live-cell imaging was performed and images were acquired every 30 s. Shown are the mean values of five measurements for bisBenzimide H 33342, c = 89 µM, and of three measurements for all other conditions. Whereas in the case of H 33342 the cells rapidly take up the dye and fluorescence intensity reaches a plateau after ~5 min, the uptake of H 33258 proceeds at a much slower rate.

bisBenzimide-free medium after the initial labeling period, it was possible to maintain the nuclear staining to such a degree that it was still recognizable after Lowicryl embedding. Considering all aspects, the following procedure was established for our CLEM experiments: incubation of cells in medium with bisBenzimide H 33342 (c = 89 µM) for 5 min at 37 °C and 5% CO_2 followed by washout of the dye. Thus, we established a straightforward nuclear staining protocol that simplifies the identification of cells within Lowicryl sections and enables the easy orientation during fluorescence and electron microscopy.

4.2 High-pressure freezing is the fixation method of choice for on-section CLEM

In order to determine what fixation protocol was optimally suited to preserve both the fluorescence signals and ultrastructural details, we compared high-pressure frozen with chemically fixed cells. For that purpose a RPE1 cell line producing fusion proteins between GFP and Centrin1, and between mCherry and the M2 mutant of Smoothened and miniSOG was investigated. The workflow for all CLEM

experiments performed in the present study is based on the *Kukulski protocol* (Kukulski et al., 2011, 2012) but was adapted to the use of STEM tomography (Fig. 2).

The preservation of the fluorescence intensity of fluorescent proteins in resin sections after dehydration at room temperature is problematic due to protein denaturation during sample preparation for electron microscopy. It was shown that the extent of fixation with formaldehyde is pH-dependent because a fixative solution with an alkaline pH leads to a higher degree of protein cross-linking than a solution with a lower pH (Berod, Hartman, & Pujol, 1981). Therefore the fluorescence preservation of the above-mentioned three fluorescent proteins was not only compared after high-pressure freezing/freeze-substitution and chemical fixation/progressive lowering of temperature but also the influence of the pH during chemical fixation was examined. For that purpose, one set of coverslips was used for fluorescence microscopy only, whereas the cells on other coverslips (and those on sapphire discs) were embedded in Lowicryl HM20 before being subjected to fluorescence microscopy. The number of fluorescent nuclei, fluorescent centrosomes and fluorescent cilia were counted and percentages were calculated. As a stably expressing cell line was used, prior to resin embedding almost all cells (∼98%) showed a Centrin1-GFP signal and ∼73–83% of Centrin1-GFP-positive cells showed an mCherry-positive cilium after 72 h of serum starvation. Results of fluorescence preservation in Lowicryl sections are shown in Fig. 3. It has to be taken into account that the percentages for the non-embedded cells are based on images of intact cells. In Lowicryl HM20 sections, however, only the basal compartments are present which we estimate to represent ∼15–20% of the total cellular volume (Fig. 3A–I). Therefore both situations are not directly comparable. After high-pressure freezing about 59.1% of nuclei were associated with a Centrin1-GFP signal and 35.0% of centrosomes with a mCherry-positive cilium (Fig. 3J and K). There appears to be a more pronounced decline in the number of fluorescent cilia compared to fluorescent centrosomes within resin sections. We conclude that chemical fixation weakens the fluorescence signal even more because the number of nuclei associated with a Centrin1-GFP signal was further reduced to 33.7% upon chemical fixation (FA, pH 7.4), and this also was the case for the number of centrosomes associated with a mCherry-positive cilium which dropped to 27.6% in chemically fixed cells (Fig. 3J and K). For reasons we do not understand we also observed a lower signal-to-noise ratio when the GFP-positive cells were imaged. However, this was not the case when we analyzed the mCherry-positive cells. A more alkaline pH did not improve fluorescence preservation, it rather caused an additional reduction of fluorescence signals for both GFP and mCherry (Fig. 3J and K).

The preservation of the cellular ultrastructure of high-pressure frozen or chemically fixed cells was validated by transmission electron microscopy on 80–90 nm thick Lowicryl sections based on the following criteria: detectability of cristae structure of mitochondria, of the double membrane of the nuclear envelope, of cytosolic membrane structures (e.g., Golgi apparatus or vesicles) and of the cytoskeleton. Whereas the cytoskeleton (mainly actin filaments) was preserved with all fixation

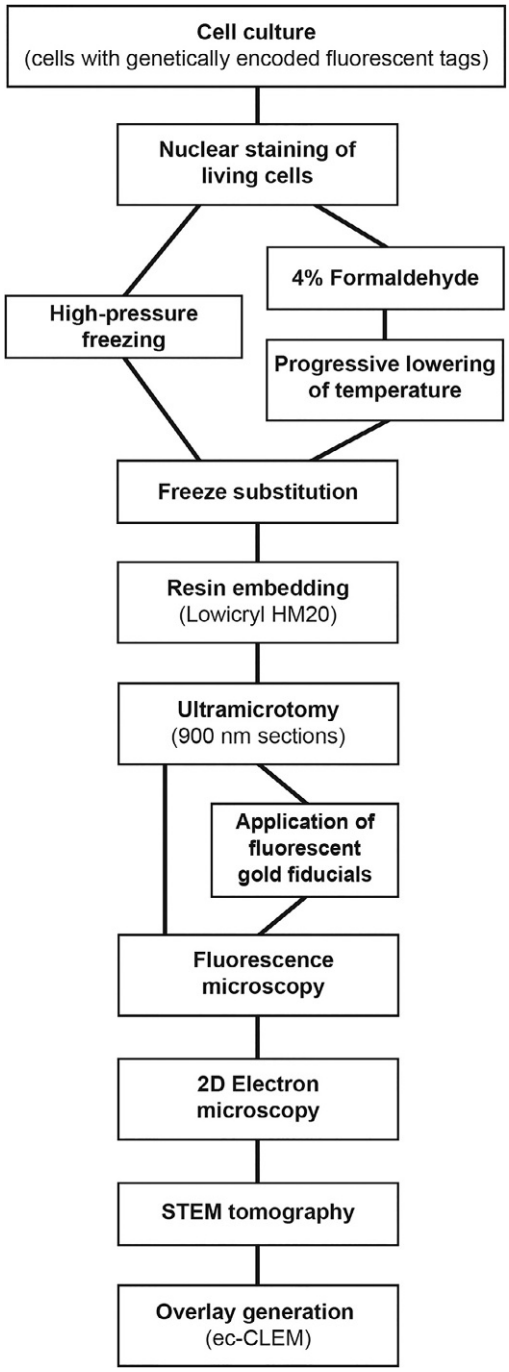

FIG. 2

Schematic overview of the workflow for the on-section CLEM-STEM approach employed in the current study. The procedure is similar to the method published previously (Kukulski et al., 2011) but each step has been adapted to the RPE1 cells and the use of the STEM technique with an electron beam of a small convergence angle. Fluorescent gold fiducials were only used when no suitable internal landmarks were present.

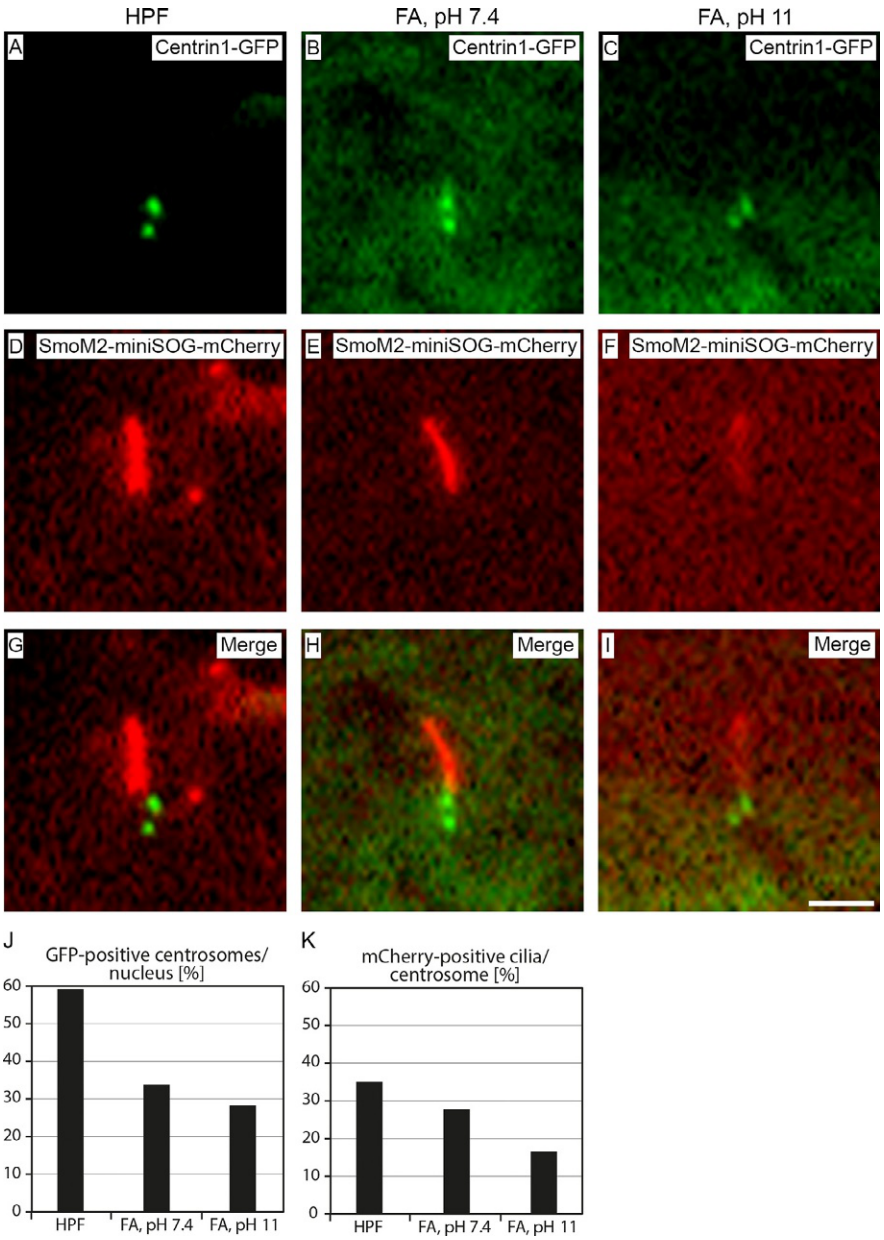

FIG. 3

See figure legend on next page.

techniques, the remaining criteria were only met in high-pressure frozen cells and never in chemically fixed ones (Fig. 4). A more alkaline pH of the formaldehyde-based fixative did not improve ultrastructural preservation.

4.3 STEM tomography is a useful tool for investigating the ultrastructure of primary cilia

As primary cilia are structures with about 300 nm in diameter and up to several microns in length (Pedersen, Schrøder, Satir, & Christensen, 2012; Witzgall, 2018), and because their components, e.g., distal and subdistal appendages, lie closely adjacent to each other (Pedersen et al., 2012), CLEM is an important tool for cilia research. To investigate large cellular structures in 3D with a resolution in the nanometer range, a STEM tomography approach with an electron beam of a small convergence angle was established in our laboratory (Rachel et al., 2020). By combining this STEM technique with on-section CLEM, fluorescently tagged proteins of interest can be localized and the associated structures can be described three-dimensionally in a volume of at least $2.7 \times 2.7 \times 0.5\,\mu m$.

For applying the established on-section CLEM-STEM workflow (Fig. 2) to the characterization of cilia, the RPE1 cells producing the fusion proteins Centrin1-GFP and SmoM2-miniSOG-mCherry were used. Regions of Lowicryl sections containing cells could easily be identified by fluorescence microscopy due to nuclear staining with bisBenzimide H 33342. The nuclear staining also facilitated orientation during overlay generation. Especially Centrin1-GFP signals could easily be assigned to their respective cells, and specific signals of fluorescent proteins could be distinguished from signals caused by impurities of the resin sections (Figs. 5A, 6A and 7A). Identifying the positions previously documented by fluorescence microscopy

FIG. 3 Comparison of fluorescence preservation after high-pressure freezing (HPF)/freeze-substitution with chemical fixation using formaldehyde (FA)/progressive lowering of temperature, followed by resin embedding. Shown are Lowicryl HM20 sections of RPE1 cells stably expressing the fusion proteins Centrin1-GFP and SmoM2-miniSOG-mCherry. Cells were serum-starved for 72 h, stained with bisBenzimide H 33342, fixed according to three different protocols (HPF, chemical fixation with formaldehyde at pH 7.4 or pH 11) and further processed as described in Fig. 2. (A–I) Representative fluorescence images of Lowicryl HM20 sections on carbon-coated finder grids. (J and K) Quantification of the percentage of fluorescent centrosomes and primary cilia. The number of GFP-positive centrosomes was related to the number of fluorescent nuclei, and the number of mCherry-positive primary cilia to the number of GFP-positive centrosomes in Lowicryl HM20 sections. $n = 180$ (HPF), $n = 253$ (FA, pH 7.4) and $n = 214$ (FA, pH 11) nuclei. $n = 105$ (HPF), $n = 84$ (FA, pH 7.4) and $n = 59$ (FA, pH 11) centrosomes. The quantification demonstrates the superior preservation of fluorescence signals after high-pressure freezing/freeze-substitution. Scale bar, 2 μm.

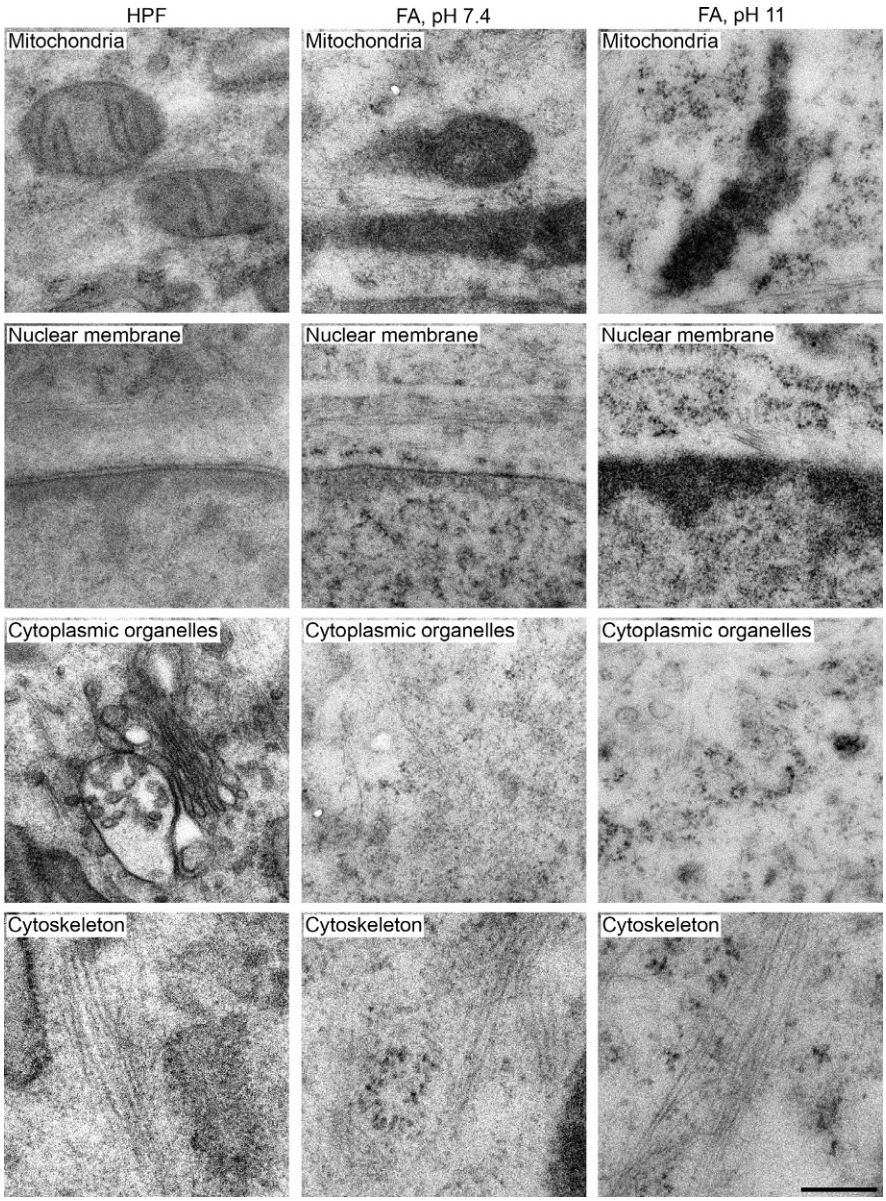

FIG. 4

Comparison of ultrastructural preservation after high-pressure freezing (HPF)/freeze-substitution with chemical fixation using formaldehyde (FA)/progressive lowering of temperature, followed by resin embedding. Shown are Lowicryl HM20 sections of RPE1 cells stably expressing the fusion proteins Centrin1-GFP and SmoM2-miniSOG-mCherry. Cells were serum-starved for 72 h, stained with bisBenzimide H 33342, fixed according to three different protocols (HPF, chemical fixation with formaldehyde at pH 7.4 or pH 11) and further processed as described in Fig. 2. Representative transmission electron micrographs of 80–90 nm thick Lowicryl HM20 sections on Pioloform-coated slot grids are shown. The preservation of the cellular ultrastructure was validated based on the detectability of cristae in mitochondria, of the double membrane of the nuclear envelope, of cytosolic membrane structures and of the cytoskeleton. The micrographs demonstrate the superior preservation of cellular structures after high-pressure freezing/freeze-substitution. Scale bar, 200 nm.

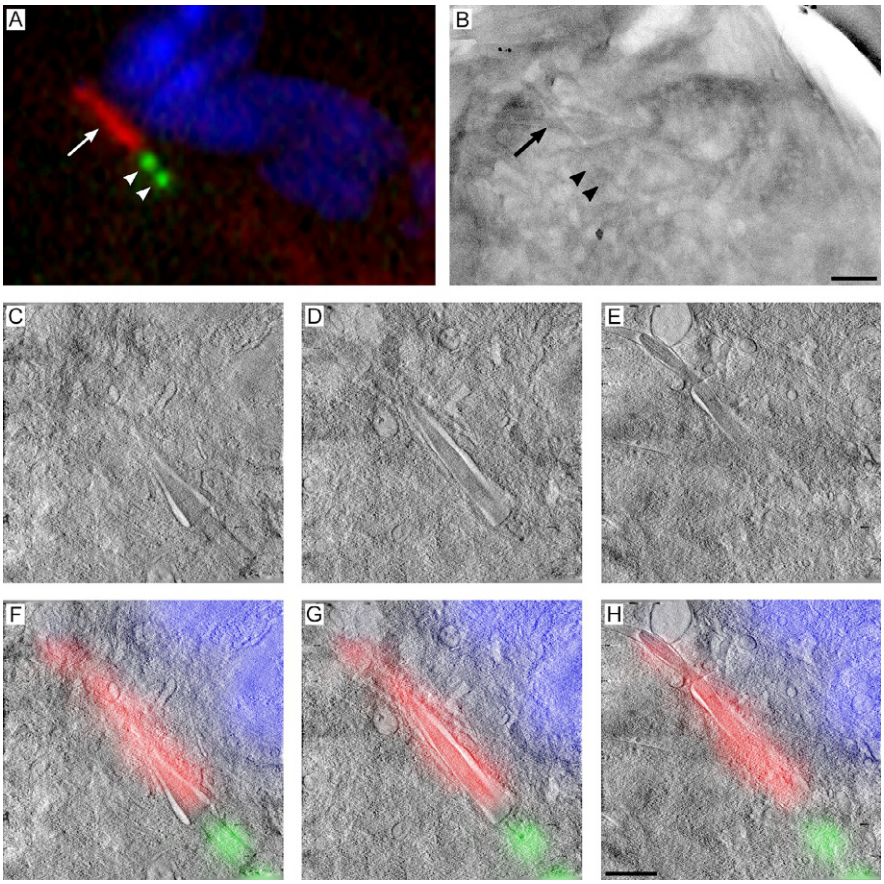

FIG. 5

On-section CLEM of high-pressure frozen RPE1 cells constitutively producing fusion proteins of Centrin1 with GFP, and of the M2 mutant of Smoothened with miniSOG and mCherry. Cells were serum-starved for 72 h to induce ciliogenesis, stained with bisBenzimide H 33342, high-pressure frozen and further processed as described in Fig. 2. (A) Fluorescence image of a Lowicryl HM20 section on a carbon-coated finder grid. The two centrioles (Centrin1-GFP, green) are marked with arrowheads, the cilium (SmoM2-miniSOG-mCherry, red) with an arrow. (B) STEM micrograph (bright-field) of the same section as in Panel (A) (centrioles marked by arrowheads, cilium marked by arrow). (C–E) At the region of interest, a tilt series of 63 images (−58° to +46°) was recorded in STEM bright-field mode. Shown are three slices of the STEM tomogram after reconstruction using the simultaneous iterative reconstruction technique (SIRT) with 15 iterations. The three slices (each with a thickness of 1.34 nm) lie ∼88 nm apart from each other in *z*. (F–H) An overlay of the fluorescence image shown in Panel (A) and of the respective slices shown in Panels (C–E) using the eC-CLEM software (Icy plugin). Scale bars, 1 μm (A and B), 500 nm (C–H).

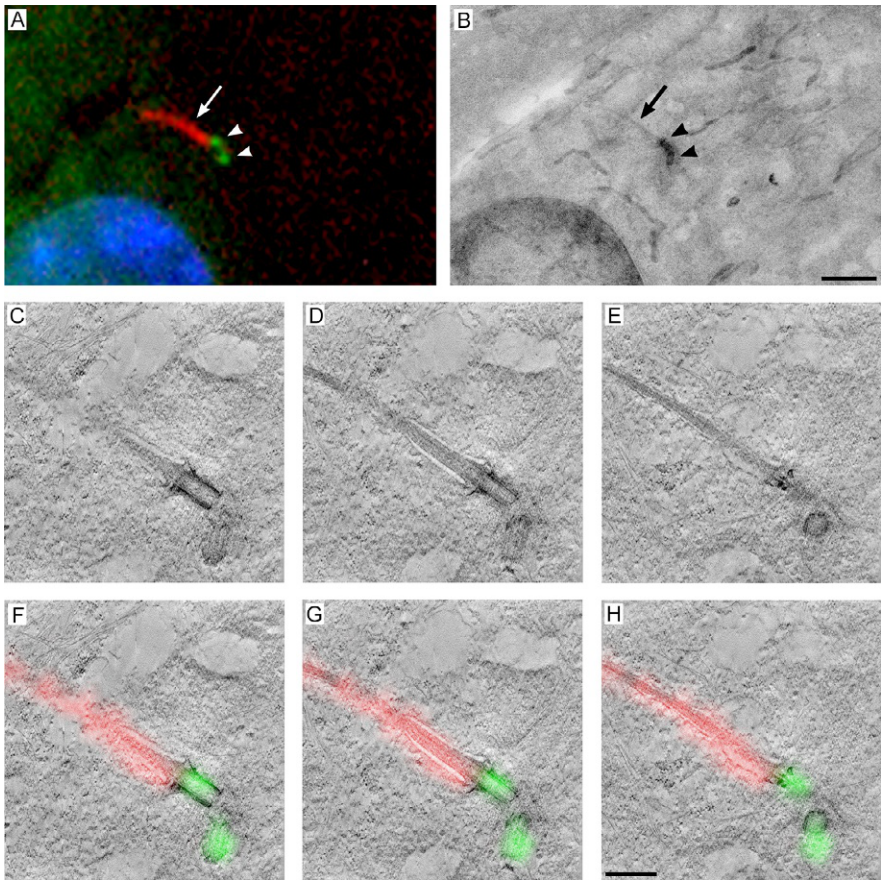

FIG. 6

On-section CLEM of RPE1 cells fixed with formaldehyde at pH 7.4 constitutively producing fusion proteins of Centrin1 with GFP, and of the M2 mutant of Smoothened with miniSOG and mCherry. Cells were serum-starved for 72 h to induce ciliogenesis, stained with bisBenzimide H 33342, fixed with formaldehyde at pH 7.4 and further processed according to the progressive lowering of temperature approach. (A) Fluorescence image of a Lowicryl HM20 section on a carbon-coated finder grid. The two centrioles (Centrin1-GFP, green) are marked with arrowheads, the cilium (SmoM2-miniSOG-mCherry, red) with an arrow. (B) STEM micrograph (bright-field) of the same section as in Panel (A) (centrioles marked by arrowheads, cilium marked by arrow). (C–E) At the region of interest, a tilt series of 90 images (−66° to +66°) was recorded in STEM bright-field mode. Shown are three slices of a STEM tomogram after reconstruction using the simultaneous iterative reconstruction technique (SIRT) with 15 iterations. The three slices (each with a thickness of 1.34 nm) lie ∼44 nm apart from each other in *z*. (F–H) An overlay of the fluorescence image shown in Panel (A) and of the respective slices shown in Panels (C–E) using the eC-CLEM software (Icy plugin). Scale bars, 2 μm (A and B), 500 nm (C–H).

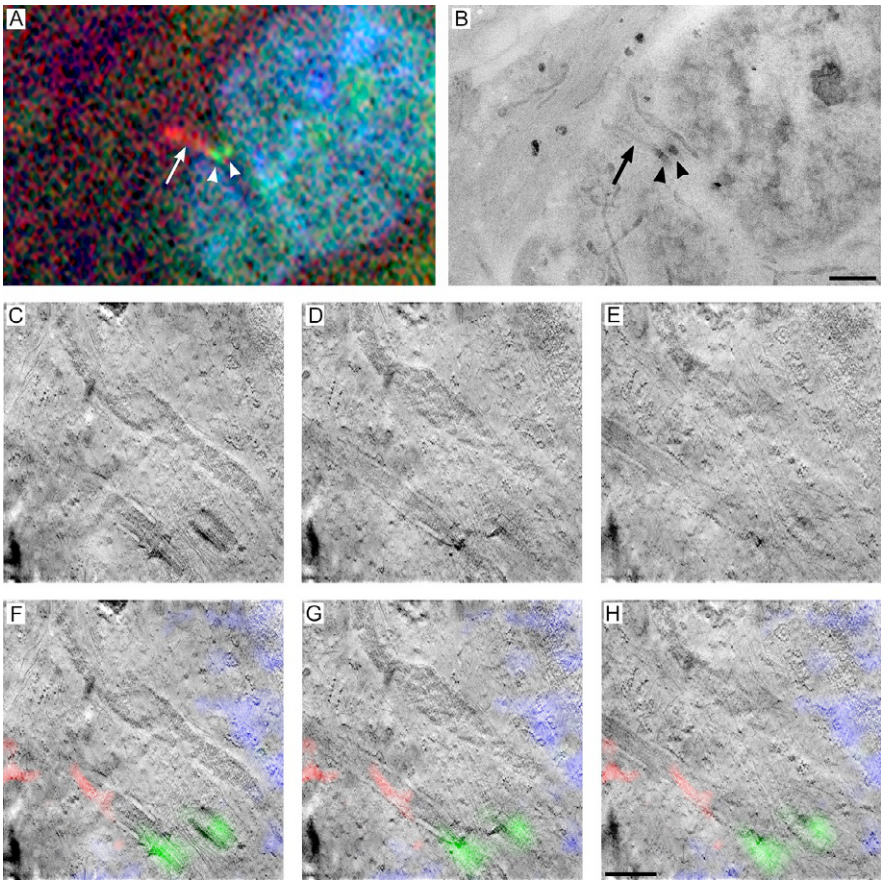

FIG. 7

On-section CLEM of RPE1 cells fixed with formaldehyde at pH 11 constitutively producing fusion proteins of Centrin1 with GFP, and of the M2 mutant of Smoothened with miniSOG and mCherry. Cells were serum-starved for 72 h to induce ciliogenesis, stained with bisBenzimide H 33342, fixed with formaldehyde at pH 11 and further processed according to the progressive lowering of temperature approach. (A) Fluorescence image of a Lowicryl HM20 section on a carbon-coated finder grid. The two centrioles (Centrin1-GFP, green) are marked with arrowheads, the cilium (SmoM2-miniSOG-mCherry, red) with an arrow. (B) STEM micrograph (bright-field) of the same section as in Panel (A) (centrioles marked by arrowheads, cilium marked by arrow). (C–E) At the region of interest, a tilt series of 78 images (−54° to +66°) was recorded in STEM bright-field mode. Shown are three slices of a STEM tomogram after reconstruction using the simultaneous iterative reconstruction technique (SIRT) with 15 iterations. The three slices (each with a thickness of 1.34 nm) lie ~44 nm apart from each other in *z*. (F–H) An overlay of the fluorescence image shown in Panel (A) and of the respective slices shown in Panels (C–E) using the eC-CLEM software (Icy plugin). Scale bars, 2 μm (A and B), 500 nm (C–H).

was straightforward. Firstly, operating the JEM-2100F electron microscope in TEM mode allowed to scan large areas faster than in STEM mode. And secondly, the software TvipsCLEM was installed directly on one of the computers operating the microscope, thus making it possible to create an approximate overlay of the fluorescence data with the ultrastructural image directly at the electron microscope. Once the regions documented by fluorescence microscopy were identified using the fluorescent nuclei and the Centrin1-GFP signals as internal landmarks, documentation was performed using the bright-field STEM mode of the microscope (Figs. 5B, 6B and 7B). In the subsequent STEM tomography (electron beam with small convergence angle) it was possible to visualize a large volume of the primary cilium including the centrosome (Figs. 5C–E, 6C–E and 7C–E) because the volumes of reconstructed tomograms were about $2.7 \times 2.7\,\mu m$ in x and y and between 330 and 400 nm in z (see Section 5.2). In reconstructed tomograms the thickness in z was always less than the 900 nm nominal thickness set at the ultramicrotome. The ultrastructure of the axoneme (which is the microtubule core of the cilium), the ciliary pocket membrane and the ciliary membrane were preserved with all fixation methods (i.e., also after chemical fixation/progressive lowering of temperature). Other membrane structures in the surrounding cytosol, however, were only visible after high-pressure freezing/freeze-substitution. This is consistent with findings presented in Section 4.2. Finally, overlays of fluorescent images and STEM tomograms were feasible without the application of additional fluorescent fiducial markers because the bisBenzimide H 33342-positive nuclei in combination with the Centrin1-GFP-positive centrosomes and the SmoM2-mCherry-positive cilia could be used as internal landmarks (Figs. 5F–H, 6F–H and 7F–H). The generation of overlays was straightforward because primary cilia are present only once per cell.

4.4 On-section CLEM-STEM in combination with fluorescently labeled gold nanoparticles can be used to investigate endosomes

The "endosomal system" consists of different compartments and is present as multiple membranous organelles within the cytoplasm (Klumperman & Raposo, 2014). Since these structures are not necessarily in close proximity to the nucleus or the centrosome, internal landmarks are not sufficient for overlay generation and additional landmarks such as electron-dense fluorescent beads are needed. They are applied to the resin sections and can be visualized by both fluorescence and electron microscopy. In the present study, rhodamine B-labeled gold nanoparticles were used (Fokkema et al., 2018). These particles have a gold core of 15 nm diameter surrounded by a silica shell extending to a diameter of 100 nm. Fluorescence intensity (Fig. 8A), electron density (Fig. 8B–D) and size (Fig. 8C and D) of these particles are ideally suited to be combined with thick resin sections during on-section CLEM-STEM experiments.

Fibroblast growth factor receptors (FGFRs) are integral membrane proteins of the plasma membrane which traffic through the endosomal system after internalization (Csanaky, Hess, & Klimaschewski, 2019). To elucidate in which organelles the

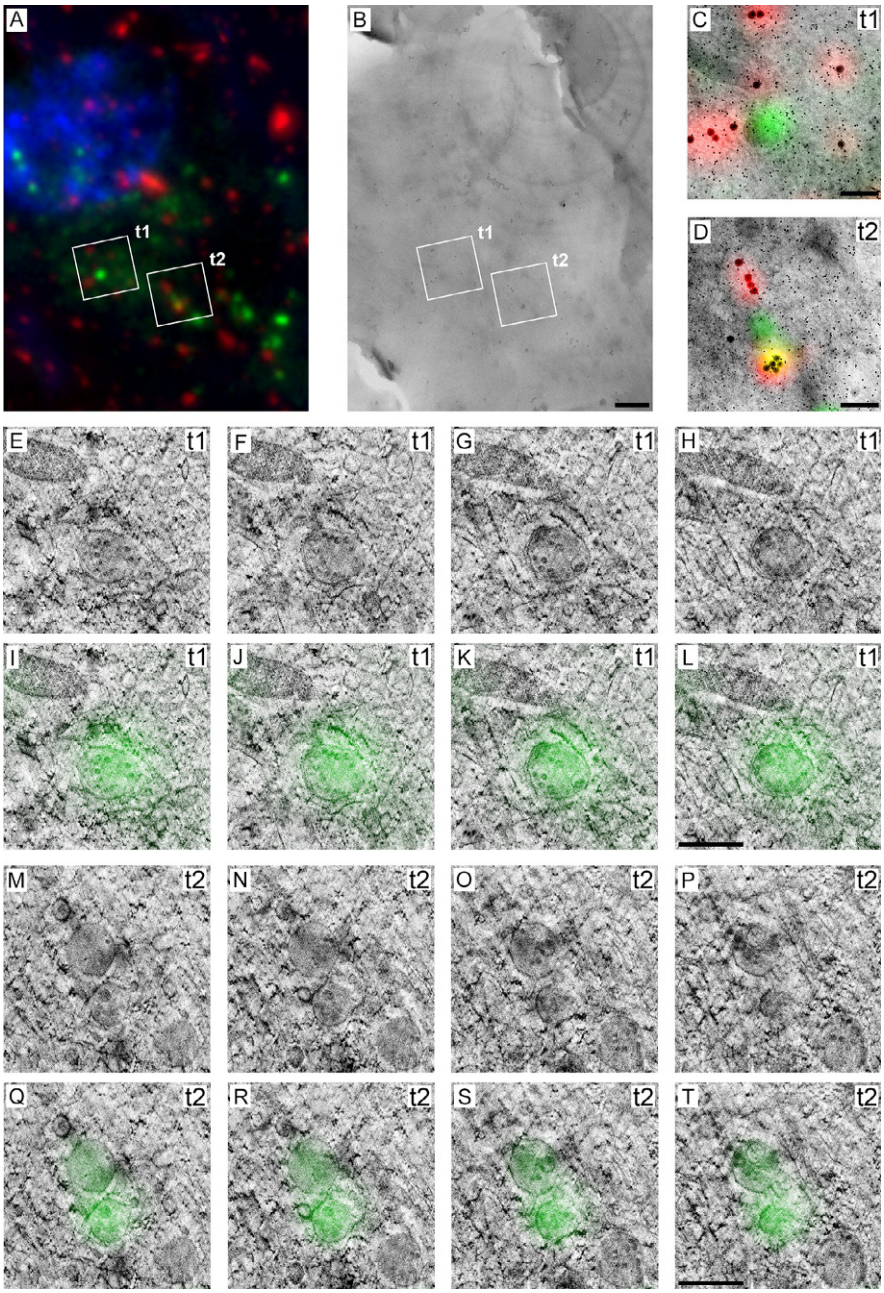

FIG. 8

See figure legend on opposite page.

receptors are located in the presence of growth factors the on-section CLEM-STEM technique proved very helpful. Twenty-four hours after plating, wild-type RPE1 cells were transiently transfected with an expression plasmid encoding a fusion protein of the FGF receptor 1 with mNeonGreen and further processed according to the workflow shown in Fig. 2. This workflow preserved the fluorescence signal of the mNeonGreen-FGFR1 fusion protein in Lowicryl sections both after high-pressure freezing (Fig. 8A) and chemical fixation with FA at pH 7.4 and 11 (images not shown). The mNeonGreen signals were distributed over the entire cytoplasm as green dots (Fig. 8A). Using the signals from nuclear staining and fluorescently labeled gold nanoparticles, positions selected by fluorescence microscopy could be identified and documented by electron microscopy (Fig. 8B). For reasons we do not understand, we observed regions where the fluorescent fiducial markers remained attached to the Lowicryl sections during fluorescence microscopy, whereas in other areas the fiducial markers moved while recording z stacks. Overlays of fluorescent images and 3D STEM data could successfully be generated with the eC-CLEM software using these beads (Fig. 8C and D), and the correlation accuracy was determined to be between about 100 and 120 nm based on the analysis of the STEM tomograms. The volumes of reconstructed tomograms were about $2.7 \times 2.7\,\mu m$ in x and y and between 240 and 540 nm in z, and therefore less than the 900 nm nominal thickness set at the ultramicrotome. In high-pressure frozen/freeze-substituted cells, mNeonGreen-FGFR1 signals were located in membrane-bound organelles containing a variable number of small vesicles (Fig. 8E–T), thus making them easily identifiable as multivesicular bodies, i.e., late endosomes (Klumperman & Raposo, 2014). Therefore the CLEM-STEM technique can be

FIG. 8 On-section CLEM of high-pressure frozen RPE1 cells producing a fusion protein of the FGF receptor 1 with mNeonGreen. RPE1 cells were transiently transfected with the expression plasmid, stained with bisBenzimide H 33342 24 h after transfection, high-pressure frozen and further processed as described in Fig. 2. (A) Fluorescence image of a Lowicryl HM20 section on a carbon-coated finder grid. Rhodamine B-labeled gold nanoparticles (Fokkema et al., 2018) were applied to the resin sections prior to imaging. The regions at which the two tilt series t1 and t2 (each 90 images, −66° to +66°) were recorded are marked with white squares. (B) STEM micrograph (bright-field) of the same section as in Panel (A). (C and D) Overlay of the fluorescence image shown in Panel (A) and of the STEM micrograph (bright-field) shown in Panel (B) of regions t1 (C) and t2 (D). The Rhodamine B-labeled gold nanoparticles were used as markers for fiducial-based correlation together with the eC-CLEM software (Icy plugin). (E–T) Shown are four slices (each with a thickness of 1.34 nm) of the STEM tomograms t1 and t2 after reconstruction using the simultaneous iterative reconstruction technique (SIRT) with 15 iterations. The four slices in Panels (E–L) and (M–T) lie ~26–31 nm apart from each other in z, respectively. Panels (E–H) and (M–P) show the slices without, Panels (I–L) and (Q–T) show the slices with the fluorescence signal. Scale bars, 2 μm (A and B), 500 nm (C, D, E–L, M–T).

extended to other fields of investigation by applying fluorescently labeled gold nanoparticles onto Lowicryl sections as fiducial markers, in particular concerning the investigation of cellular structures that appear at multiple locations.

5 Discussion

A variety of different CLEM approaches have been published in the last two decades which come with their respective advantages and disadvantages (de Boer et al., 2015; Karreman et al., 2016; Kukulski et al., 2011; Markert et al., 2016; Peddie et al., 2017; Sartori-Rupp et al., 2019). The choice of an appropriate method depends on the question to be answered. Here we developed a CLEM technique that allows the visualization of cellular structures up to several hundred nanometers in size with a high resolution in z.

5.1 Preservation of fluorescence signals and cellular ultrastructure

A crucial decision in performing CLEM experiments concerns the identification of the optimal fixation protocol. Cells and tissues can be fixed either chemically or by cryo-immobilization. Cryo-immobilization (e.g., high-pressure freezing) has become the fixation method of choice (Kaech & Ziegler, 2014) because cells and tissues are fixed in a "near-native state" (McDonald, 2009) which results in the best ultrastructural preservation so far (Kaech & Ziegler, 2014). Therefore high-pressure freezing is often used in combination with CLEM (Kukulski et al., 2011) but it can be challenging to establish conditions at which the ultrastructure of the cells is optimally preserved (McDonald et al., 2010).

Both the preservation of the cellular ultrastructure and fluorescence preservation are crucial when performing on-section CLEM experiments. Lowicryl HM20 is a suitable resin for on-section CLEM experiments as it can be polymerized below 0 °C (Carlemalm et al., 1982) which helps to preserve fluorescence (Bykov, Cortese, Briggs, & Bartenschlager, 2016; Kukulski et al., 2012). Kukulski et al. showed that red fluorescent proteins (such as mCherry) have a higher photostability than GFP after embedding in Lowicryl HM20 (Kukulski et al., 2012). The main reason for the reduced intensity of fluorescent proteins in resin sections may not be their poor structural preservation but rather their protonation during methacrylate-based resin embedding (Xiong et al., 2014). Along this line, a possible explanation for the higher photostability of red fluorescent proteins in Lowicryl sections could be that due to their lower pK_a values they are not as easily protonated as GFP (Bykov et al., 2016; Cranfill et al., 2016; Shinoda, Shannon, & Nagai, 2018). In our experiments, however, we observed a worse fluorescence preservation of mCherry than of GFP after Lowicryl embedding. We readily admit that in our study we did not fuse the proteins localizing to the same organelle with the respective fluorescent proteins. mCherry was used to tag SmoM2 which is located in the ciliary membrane (Lu et al., 2015), whereas GFP was used to tag Centrin1 which is present within the centrioles (Paoletti, Moudjou, Paintrand, Salisbury, & Bornens, 1996). Furthermore, expression levels of both fusion proteins might have been different.

Therefore a conclusion whether GFP or mCherry has a higher photostability in Lowicryl HM20 sections is not possible from our data. Finally, it should be mentioned that fluorescence intensity is lost not only after chemical fixation but also after high-pressure freezing. Independent of the fluorescent protein used, on-section CLEM is only applicable if the fluorescence signals are sufficiently bright to start with. Signals of weakly fluorescent proteins (e.g., miniSOG) are not preserved in Lowicryl sections to an extent which is necessary to visualize them even with extremely sensitive cameras.

5.2 Internal landmarks and fluorescent fiducial markers for on-section CLEM

Besides sample preparation, the overlay of fluorescent and ultrastructural pictures is another crucial step in CLEM experiments. In order to create a precise and unbiased overlay, landmarks are required which can be visualized both by light and electron microscopy. If possible, certain cellular structures can be used as internal landmarks. In case such internal landmarks are missing, fluorescent and electron-dense fiducial markers can be applied to the resin sections prior to fluorescence microscopy.

The nucleus represents such a possible internal landmark. Nuclear staining with fluorescent dyes not only allows the nuclei to be used for approximate overlay generation (Markert et al., 2016) but it also simplifies orientation on Lowicryl sections during fluorescence microscopy as shown in our study. It is possible to identify cellular structures in resin sections using bright-field light microscopy (Kukulski et al., 2012) but in contrast to fluorescent nuclear staining this requires more experience. There are two different approaches to accomplish nuclear staining, i.e., staining of live or fixed cells. To stain nuclei after fixation, various fluorescent dyes can be added to the freeze-substitution cocktail (Lucas, Günthert, Gasser, Lucas, & Wepf, 2012). However, careful establishment is required as fluorescent dyes behave differently depending on the tissue or cell line (Lucas et al., 2012). Nuclei can also be stained in resin sections with Hoechst dyes (Markert et al., 2016). In our hands, however, Lowicryl HM20 sections did not lie flat on the grids and rather showed some wrinkles. Since the dye seemed to be enriched within these wrinkles this resulted in prominent staining artifacts and made this approach impractical. To stain living cells, membrane-permeable dyes are required and fluorescence must be preserved during high-pressure freezing, freeze-substitution and Lowicryl embedding. A disadvantage of this approach is that living cells are exposed to a toxic substance which can cause artifacts. We were able to determine an appropriate incubation period that provides a bright fluorescence signal, at the same time exposing the cells as short as possible to the dye. The *Kukulski protocol* allowed to preserve the fluorescence signal of bisBenzimide H 33342 in Lowicryl HM20 sections.

Fluorescent nuclei and fluorescent centrosomes as the only internal landmarks allow merely a rough overlay of the fluorescent and ultrastructural images. If high-precision overlays with an accuracy better than 0.5 µm are required (de Boer et al., 2015), additional fluorescent fiducial markers are necessary in most cases. Due to the thick resin sections analyzed by STEM tomography in this study,

fluorescent fiducial markers had to contain a sufficiently electron-dense core to be imaged by electron microscopy. For this reason, commercially available particles (e.g., FluoSpheres, Thermo Fisher Scientific) with a polymer core proved unsuitable. Fluorescently labeled and silica-coated gold nanoparticles can easily be imaged by electron microscopy because of their gold core (Fokkema et al., 2018). Furthermore they show a sufficiently bright fluorescence so that individual particles can be identified by fluorescence microscopy, and there are no further steps required as with, e.g., FluoSpheres which must first be washed with 1× PBS/0.1% Tween-20 (Kukulski et al., 2012). Theoretically, the nanoparticles can even be used for tomogram reconstruction. However, the software IMOD had problems to generate artifact-free reconstructions using only the silica-coated gold nanoparticles which is probably due to the fact that only few gold nanoparticles were present in the region to be reconstructed for tomography. Obviously it is necessary to apply gold fiducials to both sides of the grid, especially on thick resin sections (remember that fluorescent fiducial markers for CLEM are typically applied only to one side of a grid). In addition, the silica-coated gold nanoparticles cannot be used at high concentrations since they tend to clump and therefore cannot be visualized as separate particles due to the limited resolution of fluorescence microscopy. For this reason, we recommend to also apply 15-nm colloidal protein A-gold particles which are better suited for tomographic reconstruction using IMOD. On the downside, the application of protein A-gold particles to the Lowicryl section/carbon-coated finder grid assembly is not easy to accomplish. For reasons we do not understand, protein A-gold particles attach only poorly to the carbon coating of the finder grids. Highly concentrated particle solutions, plasma cleaning or covering the grids, e.g., with FCS, did not improve the attachment of the protein A-gold particles.

Although Lowicryl HM20 sections were generated with a nominal thickness of 900 nm, the actual thickness of reconstructed tomograms in z was 240–540 nm only. One explanation for this discrepancy lies in the fact that we typically used the very first section from our embedded cells because the structures of interest (centrosomes and cilia) are located in the basal compartment of RPE1 cells. This first section is inevitably thinner than the nominal setting on the control unit of the ultramicrotome. In addition, it was shown that Lowicryl HM20 sections undergo a mass loss of ∼30% during exposure to the electron beam (Kizilyaprak, Longo, Daraspe, & Humbel, 2015), thus it can be estimated that the Lowicryl sections used in the current study were between ∼340 and 770 nm thick before exposure to the electron beam. Since it was shown that it is possible to perform STEM tomography at 200 kV on up to 900 nm thick sections (Rachel et al., 2020), we believe that our CLEM-STEM approach will also work on those thicker sections.

5.3 On-section CLEM-STEM approach to study low-copy and multi-copy organelles

Our on-section CLEM-STEM technique is useful to study the biology of cilia because it allows to visualize this particular structure with its diameter of several hundreds of nm in one section. Primary cilia are singular organelles present on

almost every mammalian cell type (Anderson et al., 2008; Satir, Pedersen, & Christensen, 2010). Since primary cilia are solitary organelles, internal landmarks are sufficient to localize these structures within a cell during electron microscopy. Furthermore, overlays with the required accuracy can be achieved by simply using internal landmarks without applying fluorescent fiducial markers. In addition to nuclear staining, the centrosome serves as an additional ubiquitous internal landmark.

Each centrosome contains a mother and a daughter centriole, the former gives rise to the basal body from which the primary cilium grows out (Pedersen et al., 2012). By fusing Centrin1, which is concentrated at the distal end of both centrioles (Pihan, 2013; Uetake et al., 2007) with fluorescent proteins, the two centrioles are ideal internal landmarks for CLEM experiments. Smoothened is a G-protein-coupled receptor and contributes to the activation of the Hedgehog signaling pathway (Corbit et al., 2005; Qi et al., 2019). The constitutively active M2 mutant of Smoothened localizes to the ciliary membrane even without activation of the Hedgehog pathway and therefore serves as a ciliary marker (Incardona et al., 2002; Lu et al., 2015; Yee & Reiter, 2015). A stably expressing cell line constitutively producing the fusion proteins Centrin1-GFP and SmoM2-miniSOG-mCherry was used in the present study. The SmoM2-miniSOG-mCherry fusion protein was located at the primary cilium. Since the ciliary membrane and the pocket membrane lie only a few nanometers apart in RPE1 cells, it was not possible to distinguish whether Smoothened localizes not only to the ciliary membrane but also to the pocket membrane. To get more detailed information it would be necessary to combine on-section CLEM with super-resolution microscopy (Johnson et al., 2015).

Having shown that our CLEM approach is suitable for investigating singular organelles such as the centrosome or the primary cilium, we expanded the range of applications to examine structures that are present at multiple locations within a cell. It was possible to localize the FGF receptor 1 in multivesicular bodies, thus demonstrating the use of our method for further biological applications.

6 Conclusion

We have established an on-section CLEM approach which can be used to identify fluorescently tagged proteins in resins and to visualize the underlying ultrastructure up to a volume of at least $2.7 \times 2.7 \times 0.5\,\mu m$. To investigate singular organelles such as the nucleus, the centrosome or the primary cilium, internal landmarks are sufficient to generate an unbiased overlay. We recommend the application of additional fluorescent fiducial markers for reliable overlay generation if organelles are studied that are present in multiple copies such as mitochondria and endosomes. Our on-section CLEM approach in combination with STEM tomography will be useful to analyze a variety of organelles occupying large cellular volumes.

Acknowledgments

We thank Lars Klimaschewski (Medical University of Innsbruck, Austria), Rajat Rohatgi (Stanford University, USA) and Gislene Pereira (Center for Organismal Studies, University of Heidelberg, Germany) for sharing reagents. Ruediger Eder and Irina Fink (Regensburg Center for Interventional Immunology, University Hospital Regensburg) kindly performed the FACS analysis. We also thank Anthonie Maurer, Larissa Osten and Anita Zuegner (Institute for Molecular and Cellular Anatomy, University of Regensburg) for their technical support and Paul Walther (Central Facility for Electron Microscopy, University of Ulm, Germany) for discussions and proofreading the manuscript. This project was supported by the Deutsche Forschungsgemeinschaft (DFG) through SFB 699 and 1350 (to RR and RW).

References

Ader, N. R., & Kukulski, W. (2017). Triclem: Combining high-precision, room temperature CLEM with cryo-fluorescence microscopy to identify very rare events. *Methods in Cell Biology*, *140*, 303–320.

Anderson, C. T., Castillo, A. B., Brugmann, S. A., Helms, J. A., Jacobs, C. R., & Stearns, T. (2008). Primary cilia: Cellular sensors for the skeleton. *Anatomical Record*, *291*, 1074–1078.

Berod, A., Hartman, B. K., & Pujol, J. F. (1981). Importance of fixation in immunohistochemistry: Use of formaldehyde solutions at variable pH for the localization of tyrosine hydroxylase. *The Journal of Histochemistry and Cytochemistry*, *29*, 844–850.

Biel, S. S., Kawaschinski, K., Wittern, K.-P., Hintze, U., & Wepf, R. (2003). From tissue to cellular ultrastructure: Closing the gap between micro- and nanostructural imaging. *Journal of Microscopy*, *212*, 91–99.

Biskupek, J., Leschner, J., Walther, P., & Kaiser, U. (2010). Optimization of STEM tomography acquisition-a comparison of convergent beam and parallel beam STEM tomography. *Ultramicroscopy*, *110*, 1231–1237.

Bykov, Y. S., Cortese, M., Briggs, J. A. G., & Bartenschlager, R. (2016). Correlative light and electron microscopy methods for the study of virus-cell interactions. *FEBS Letters*, *590*, 1877–1895.

Carlemalm, E., Garavito, R. M., & Villiger, W. (1982). Resin development for electron microscopy and an analysis of embedding at low temperature. *Journal of Microscopy*, *126*, 123–143.

Chen, J. K., Taipale, J., Cooper, M. K., & Beachy, P. A. (2002). Inhibition of Hedgehog signaling by direct binding of cyclopamine to Smoothened. *Genes & Development*, *16*, 2743–2748.

Cockett, M. I., Ochalski, R., Benwell, K., Franco, R., & Wardwell-Swanson, J. (1997). Simultaneous expression of multi-subunit proteins in mammalian cells using a convenient set of mammalian cell expression vectors. *BioTechniques*, *23*, 402–406.

Corbit, K. C., Aanstad, P., Singla, V., Norman, A. R., Stainier, D. Y. R., & Reiter, J. F. (2005). Vertebrate Smoothened functions at the primary cilium. *Nature*, *437*, 1018–1021.

Cranfill, P. J., Sell, B. R., Baird, M. A., Allen, J. R., Lavagnino, Z., de Gruiter, H. M., et al. (2016). Quantitative assessment of fluorescent proteins. *Nature Methods*, *13*, 557–562.

Csanaky, K., Hess, M. W., & Klimaschewski, L. (2019). Membrane-associated, not cytoplasmic or nuclear, FGFR1 induces neuronal differentiation. *Cell*, *8*, 243.

de Boer, P., Hoogenboom, J. P., & Giepmans, B. N. G. (2015). Correlated light and electron microscopy: Ultrastructure lights up! *Nature Methods*, *12*, 503–513.

de Chaumont, F., Dallongeville, S., Chenouard, N., Hervé, N., Pop, S., Provoost, T., et al. (2012). Icy: An open bioimage informatics platform for extended reproducible research. *Nature Methods*, *9*, 690–696.

Fokkema, J., Fermie, J., Liv, N., van den Heuvel, D. J., Konings, T. O. M., Blab, G. A., et al. (2018). Fluorescently labelled silica coated gold nanoparticles as fiducial markers for correlative light and electron microscopy. *Scientific Reports*, *8*, 13625.

Giepmans, B. N. G. (2008). Bridging fluorescence microscopy and electron microscopy. *Histochemistry and Cell Biology*, *130*, 211–217.

Hell, S. W., & Wichmann, J. (1994). Breaking the diffraction resolution limit by stimulated emission: Stimulated-emission-depletion fluorescence microscopy. *Optics Letters*, *19*, 780–782.

Incardona, J. P., Gruenberg, J., & Roelink, H. (2002). Sonic hedgehog induces the segregation of patched and smoothened in endosomes. *Current Biology*, *12*, 983–995.

Johnson, E., Seiradake, E., Jones, E. Y., Davis, I., Grünewald, K., & Kaufmann, R. (2015). Correlative in-resin super-resolution and electron microscopy using standard fluorescent proteins. *Scientific Reports*, *5*, 9583.

Kaech, A., & Ziegler, U. (2014). High-pressure freezing: Current state and future prospects. *Methods in Molecular Biology*, *1117*, 151–171.

Karreman, M. A., Mercier, L., Schieber, N. L., Solecki, G., Allio, G., Winkler, F., et al. (2016). Fast and precise targeting of single tumor cells in vivo by multimodal correlative microscopy. *Journal of Cell Science*, *129*, 444–456.

Kizilyaprak, C., Longo, G., Daraspe, J., & Humbel, B. M. (2015). Investigation of resins suitable for the preparation of biological sample for 3-D electron microscopy. *Journal of Structural Biology*, *189*, 135–146.

Klumperman, J., & Raposo, G. (2014). The complex ultrastructure of the endolysosomal system. *Cold Spring Harbor Perspectives in Biology*, *6*, a016857.

Kobayashi, S., Serizawa, Y., Fujita, T., & Coupland, R. E. (1978). SGC (small granule chromaffin) cells in the mouse adrenal medulla: Light and electron microscopic identification using semi-thin and ultra-thin sections. *Endocrinologia Japonica*, *25*, 467–476.

Kremer, J. R., Mastronarde, D. N., & McIntosh, J. R. (1996). Computer visualization of three-dimensional image data using IMOD. *Journal of Structural Biology*, *116*, 71–76.

Kukulski, W., Schorb, M., Welsch, S., Picco, A., Kaksonen, M., & Briggs, J. A. G. (2011). Correlated fluorescence and 3D electron microscopy with high sensitivity and spatial precision. *The Journal of Cell Biology*, *192*, 111–119.

Kukulski, W., Schorb, M., Welsch, S., Picco, A., Kaksonen, M., & Briggs, J. A. G. (2012). Precise, correlated fluorescence microscopy and electron tomography of lowicryl sections using fluorescent fiducial markers. *Methods in Cell Biology*, *111*, 235–257.

Lu, Q., Insinna, C., Ott, C., Stauffer, J., Pintado, P. A., Rahajeng, J., et al. (2015). Early steps in primary cilium assembly require EHD1/EHD3-dependent ciliary vesicle formation. *Nature Cell Biology*, *17*, 228–240.

Lucas, M. S., Günthert, M., Gasser, P., Lucas, F., & Wepf, R. (2012). Bridging microscopes: 3D correlative light and scanning electron microscopy of complex biological structures. *Methods in Cell Biology*, *111*, 325–356.

Markert, S. M., Britz, S., Proppert, S., Lang, M., Witvliet, D., Mulcahy, B., et al. (2016). Filling the gap: Adding super-resolution to array tomography for correlated ultrastructural and molecular identification of electrical synapses at the *C. Elegans* connectome. *Neurophotonics*, *3*, 41802.

McDonald, K. L. (2009). A review of high-pressure freezing preparation techniques for correlative light and electron microscopy of the same cells and tissues. *Journal of Microscopy*, *235*, 273–281.

McDonald, K., Schwarz, H., Müller-Reichert, T., Webb, R., Buser, C., & Morphew, M. (2010). "Tips and tricks" for high-pressure freezing of model systems. *Methods in Cell Biology*, *96*, 671–693.

McIntosh, R., Nicastro, D., & Mastronarde, D. (2005). New views of cells in 3D: An introduction to electron tomography. *Trends in Cell Biology*, *15*, 43–51.

Mohammadian, S., Fokkema, J., Agronskaia, A. V., Liv, N., de Heus, C., van Donselaar, E., et al. (2019). High accuracy, fiducial marker-based image registration of correlative microscopy images. *Scientific Reports*, *9*, 3211.

Noske, A. B., Costin, A. J., Morgan, G. P., & Marsh, B. J. (2008). Expedited approaches to whole cell electron tomography and organelle mark-up in situ in high-pressure frozen pancreatic islets. *Journal of Structural Biology*, *161*, 298–313.

Paoletti, A., Moudjou, M., Paintrand, M., Salisbury, J. L., & Bornens, M. (1996). Most of centrin in animal cells is not centrosome-associated and centrosomal centrin is confined to the distal lumen of centrioles. *Journal of Cell Science*, *109*, 3089–3102.

Paul-Gilloteaux, P., Heiligenstein, X., Belle, M., Domart, M.-C., Larijani, B., Collinson, L., et al. (2017). eC-CLEM: Flexible multidimensional registration software for correlative microscopies. *Nature Methods*, *14*, 102–103.

Peddie, C. J., Domart, M.-C., Snetkov, X., O'Toole, P., Larijani, B., Way, M., et al. (2017). Correlative super-resolution fluorescence and electron microscopy using conventional fluorescent proteins in vacuo. *Journal of Structural Biology*, *199*, 120–131.

Pedersen, L. B., Schrøder, J. M., Satir, P., & Christensen, S. T. (2012). The ciliary cytoskeleton. *Comprehensive Physiology*, *2*, 779–803.

Pihan, G. A. (2013). Centrosome dysfunction contributes to chromosome instability, chromoanagenesis, and genome reprograming in cancer. *Frontiers in Oncology*, *3*, 277.

Qi, X., Liu, H., Thompson, B., McDonald, J., Zhang, C., & Li, X. (2019). Cryo-EM structure of oxysterol-bound human Smoothened coupled to a heterotrimeric G_i. *Nature*, *571*, 279–283.

Rachel, R., Walther, P., Maaßen, C., Daberkow, I., Matsuoka, M., & Witzgall, R. (2020). Dual-axis STEM tomography at 200 kV: Setup, performance, limitations. *Journal of Structural Biology*, *211*, 107551.

Robertson, D., Monaghan, P., Clarke, C., & Atherton, A. J. (1992). An appraisal of low-temperature embedding by progressive lowering of temperature into Lowicryl HM20 for immunocytochemical studies. *Journal of Microscopy*, *168*, 85–100.

Rueden, C. T., Schindelin, J., Hiner, M. C., DeZonia, B. E., Walter, A. E., Arena, E. T., et al. (2017). Imagej2: Imagej for the next generation of scientific image data. *BMC Bioinformatics*, *18*, 529.

Saghi, Z., & Midgley, P. A. (2012). Electron tomography in the (S)TEM: From nanoscale morphological analysis to 3D atomic imaging. *Annual Review of Materials Research*, *42*, 59–79.

Santarella-Mellwig, R., Haselmann, U., Schieber, N. L., Walther, P., Schwab, Y., Antony, C., et al. (2018). Correlative light electron microscopy (CLEM) for tracking and imaging viral protein associated structures in cryo-immobilized cells. *Journal of Visualized Experiments, 139,* e58154.

Sartori-Rupp, A., Cordero Cervantes, D., Pepe, A., Gousset, K., Delage, E., Corroyer-Dulmont, S., et al. (2019). Correlative cryo-electron microscopy reveals the structure of TNTs in neuronal cells. *Nature Communications*, *10*, 342.

Satir, P., Pedersen, L. B., & Christensen, S. T. (2010). The primary cilium at a glance. *Journal of Cell Science*, *123*, 499–503.

Saxton, W. O., Baumeister, W., & Hahn, M. (1984). Three-dimensional reconstruction of imperfect two-dimensional crystals. *Ultramicroscopy*, *13*, 57–70.

Schindelin, J., Arganda-Carreras, I., Frise, E., Kaynig, V., Longair, M., Pietzsch, T., et al. (2012). Fiji: An open-source platform for biological-image analysis. *Nature Methods*, *9*, 676–682.

Schorb, M., Gaechter, L., Avinoam, O., Sieckmann, F., Clarke, M., Bebeacua, C., et al. (2017). New hardware and workflows for semi-automated correlative cryo-fluorescence and cryo-electron microscopy/tomography. *Journal of Structural Biology*, *197*, 83–93.

Shaner, N. C., Lambert, G. G., Chammas, A., Ni, Y., Cranfill, P. J., Baird, M. A., et al. (2013). A bright monomeric green fluorescent protein derived from *Branchiostoma lanceolatum*. *Nature Methods*, *10*, 407–409.

Shinoda, H., Shannon, M., & Nagai, T. (2018). Fluorescent proteins for investigating biological events in acidic environments. *International Journal of Molecular Sciences*, *19*, 1548.

Shu, X., Lev-Ram, V., Deerinck, T. J., Qi, Y., Ramko, E. B., Davidson, M. W., et al. (2011). A genetically encoded tag for correlated light and electron microscopy of intact cells, tissues, and organisms. *PLoS Biology*, *9*, e1001041.

Sousa, A. A., & Leapman, R. D. (2012). Development and application of STEM for the biological sciences. *Ultramicroscopy*, *123*, 38–49.

Uetake, Y., Loncarek, J., Nordberg, J. J., English, C. N., La Terra, S., Khodjakov, A., et al. (2007). Cell cycle progression and de novo centriole assembly after centrosomal removal in untransformed human cells. *The Journal of Cell Biology*, *176*, 173–182.

Witzgall, R. (2018). Golgi bypass of ciliary proteins. *Seminars in Cell & Developmental Biology*, *83*, 51–58.

Xiong, H., Zhou, Z., Zhu, M., Lv, X., Li, A., Li, S., et al. (2014). Chemical reactivation of quenched fluorescent protein molecules enables resin-embedded fluorescence microimaging. *Nature Communications*, *5*, 3992.

Yang, T. T., Chong, W. M., Wang, W.-J., Mazo, G., Tanos, B., Chen, Z., et al. (2018). Super-resolution architecture of mammalian centriole distal appendages reveals distinct blade and matrix functional components. *Nature Communications*, *9*, 2023.

Yee, L. E., & Reiter, J. F. (2015). Ciliary vesicle formation: A prelude to ciliogenesis. *Developmental Cell*, *32*, 665–666.